Unraveling the heterogeneous mutational signature of spontaneously developing tumors in MLH1$^{-/-}$ mice

Yvonne Saara Gladbach [1,2,3], Leonie Wiegele [4], Mohamed Hamed [1], Anna-Marie Merkenschlager [1], Georg Fuellen [1], Christian Junghanss [4], Claudia Maletzki [4*]

[1] Rostock University Medical Center, Institute for Biostatistics and Informatics in Medicine and Ageing Research (IBIMA), Rostock, Germany

[2] Faculty of Biosciences, Heidelberg University, 69120, Heidelberg, Germany

[3] Division of Applied Bioinformatics, German Cancer Research Center (DKFZ) and National Center for Tumor Diseases (NCT) Heidelberg, 69120, Heidelberg, Germany

[4] Department of Internal Medicine, Medical Clinic III - Hematology, Oncology, Palliative Medicine; Rostock University Medical Center, University of Rostock, 18057 Rostock, Germany

Running title: Mutations in MLH1$^{-/-}$ tumors

Corresponding author:

Claudia Maletzki, PhD

Department of Internal Medicine, Medical Clinic III - Hematology, Oncology, Palliative Medicine; Rostock University Medical Center, University of Rostock, 18057 Rostock Germany

Ernst-Heydemann-Straße 6, D-18057 Rostock, Germany

claudia.maletzki@med.uni-rostock.de

Telephone: ++49 381 494 5764

Fax: ++49 381 494 5898

This work was supported by the German research foundation to CM [DFG grant number MA5799/2-1].

Abbreviations: CMMR-D – constitutional mismatch repair deficiency, cMS – coding microsatellite, MB – Megabase, MMR – mismatch repair, MMR-D – mismatch repair deficiency, TMB – tumor mutational burden, GIT – gastrointestinal tumor, SNV – single nucleotide variant, WES – whole exome sequencing

Keywords: Tumor mutational burden, exclusive/ shared mutations, predicted tumor antigens

Abstract

MLH1 knock out mice represent a preclinical model that resembles features of the human counterpart. As these mice develop mismatch repair deficient (MMR-D) neoplasias in a sequential twin-peaked manner (first lymphomas, then gastrointestinal tumors) we aimed at identification of the underlying molecular mechanisms. Using whole-exome sequencing, we focused on (I) shared and (II) mutually exclusive mutations and described the processes of ongoing mutational events in tumor-derived cultures.

A heterogeneous genetic landscape was found, with few mutations shared among different neoplasias (*ARID1A* and *IDH2*). Mutations in tumor suppressor genes *SMAD4* and *POLE* were mutually exclusive in lymphomas, most likely contributing to a more aggressive *in vivo* phenotype. Comparing the mutational profile of selected primary tumors and their corresponding cell line upon *in vitro* culture revealed continuous increased numbers of somatic gene mutations. The same was true for coding microsatellite mutations in selected MMR-D target genes, showing a gradual increase during *in vitro* passage. With respect to this latter type of mutations, partial overlap was detectable, yet recognizing shared vaccination antigens. The two most promising candidates are *AKT3*, a RAC-gamma serine/threonine-protein kinase with relevance in maintenance of cellular homeostasis and the endonuclease *ERCC5* (Excision Repair 5), involved in DNA excision repair.

Novel results of a comparison between spontaneously developing lymphomas and gastrointestinal tumors as models for MMR-D driven tumorigenesis are reported. In addition to identification of *ARID1A* as a potentially causative mutation hotspot, our comprehensive characterization of the mutational signature is a starting point for immune-based approaches to therapy.

Author Summary

This study describes the mutational spectrum of MLH1$^{-/-}$-associated tumors, spontaneously developing in mice. While these tumors arise at the bottom of the same germline mutation, the clinical presentations as well as resulting molecular alterations are heterogeneous, and thus likely being directly linked. Highly aggressive lymphomas, developing early in life are ultra-hypermutated and harbor mutations in tumor suppressor genes *SMAD4* and *POLE*. Gastrointestinal tumors develop later in life and show different mutations. By performing in-depth whole exome sequencing analysis, we here identified for the first time a common mutational hotspot. *ARID1A* constitutes a potentially causative mutation, shared among different MLH1$^{-/-}$-associated tumors and thus irrespective of the origin. Additional interesting and identified candidate genes include AKT3, a RAC-gamma serine/threonine-protein kinase and the endonuclease ERCC5. Both genes are bona fide tumor suppressors with significant relevance in DNA excision repair and maintenance of cellular homeostasis. This finding is of particular relevance for subsequent therapeutic and - even more important - prophylactic vaccination approaches aiming at entity-overlapping treatment of MLH1$^{-/-}$-related tumors.

1. Introduction

Comprehensive genomic sequencing is an increasingly common practice in oncological precision medicine. The technological improvements in analyzing diseases at the genomic, transcriptomic and epigenetic levels allow for the identification of characteristic genetic changes. To detect disease-causing variants (so-called driver mutations) and discover therapeutic target genes, whole exome sequencing (WES) is a highly fruitful sequencing method (1). By applying this method, the coding region of the genome is captured and sequenced at high depth. The interrogation of the exome in clinical diagnosis raises challenges of uncovering mutational profiles of heterogeneous tumors and may allow the development of new immunotherapeutic approaches (2,3).

Mutations in MLH1$^{-/-}$ tumors

Closely linked to hypermutation and high immunogenicity is the *MLH1* gene, belonging to the DNA mismatch-repair (MMR) family. Germline, as well as somatic *MLH1* mutations drive tumorigenesis. The hallmark of the resulting tumors are a mismatch-repair deficiency (MMR-D) and an exceedingly high tumor mutational burden (TMB) (4). The latter is characterized by frameshift mutations and, in consequence, by functionally impaired proteins as well as elevated frequencies of non-synonymous mutations. A high neoantigen load reflects high TMB. The tumor cells' MHC molecules, capable of eliciting anticancer T cell responses, present these mutated self-peptides. However, immune evasion, such as loss of the MHC class I subunit, beta-2-microglobulin as well as upregulation of immune-checkpoint molecules (PD-1/PD-L1) is quite common and most tumor-infiltrating T cells show signs of exhaustion (5).

Clinically, MMR-D is associated with sporadic as well as hereditary cancer, with the latter being due to mono- or biallelic MMR germline mutations. Individuals with monoallelic germline mutations suffer from Lynch syndrome and have an 80 % lifetime risk of developing cancer (6). The bi-allelic counterpart is constitutional mismatch-repair deficiency (CMMR-D), associated with a complex and a slightly different tumor spectrum than that seen in Lynch-associated cancers (7,8). As there is a high likelihood of tumorigenesis for both syndromes, attempts to delay or even prevent tumor formation are ongoing (e.g., *clinicaltrials.gov.identifiers*: NCT01885702; NCT02813824; NCT02497820; NCT03070574). Moreover, preclinical tumor models may provide new insights into tumor biology, helping to refine prevention and therapy.

MLH1$^{-/-}$ knockout mice constitute an ideal preclinical model for hereditary tumor syndromes. With a virtually 100 % penetrance, these mice develop a variety of malignancies, including highly aggressive lymphomas in different organ sites, gastrointestinal tumors, and malignant skin lesions (9,10). The sequential appearance of these neoplasias, often in a mutually

exclusive fashion ("either-or" principle in terms of tumor type) raises the question of how the biological and/or molecular mechanisms of these neoplasias relate to each other. To gain insights into the underlying molecular alterations that affect tumor formation and thus act as drivers, we herein analyzed the number and type of somatic mutations arising at the bottom of a germline MMR-D. Exclusive as well as shared alterations were identified, explaining the heterogeneous clinical presentation.

2. Results

2.1. *In vivo* and *ex vivo* data

MLH1$^{-/-}$ mice are prone to different tumors. Data from 90 mice reveal a heterogeneous distribution pattern and the median age of onset varies, with a high prevalence of early Non-Hodgkin T cell lymphomas, primarily arising in the thymus and spleen (43.5 and 18.5 %, respectively), after which mice develop epithelial tumors of the gastrointestinal tract (GIT), primarily located in the duodenum or lymphoid skin lesions (26.0 and 12.0 %, respectively). Besides, gender-specific differences are apparent with female mice developing lymphomas more frequently than GIT and *vice versa* in males (Figure 1A).

For our comprehensive analysis, we included a set of four tumor samples, mainly covering the spectrum observed in MLH1$^{-/-}$ mice (Table 1). Since all MLH1$^{-/-}$-associated tumors harbor MHC class I on their surface, which is preserved in the resulting *in vitro* cell culture as well as in the allograft (9), phenotyping focused on immune evasion markers, such as PD-L1, CTLA-4, LAG-3, and TIM-3. As anticipated, lymphomas expressed all markers in high abundance (Figure 1B). By contrast, PD-L1 and CTLA-4 surface expression on GIT was heterogeneous and found on only 20-40 % of cells, respectively (Figure 1B; referring to P11 and P12, respectively). LAG-3 and TIM-3 expression was confined to tumor-infiltrating lymphocytes and thus below 5 % (Figure 1B; referring to P14 and P15, respectively and (11)). Generally, lymphocytic infiltrates in MLH1$^{-/-}$-associated GIT showed an equal distribution between CD3^{+}CD4^{+} and CD3^{+}CD8^{+} T cells (Figure 1C, right bars with dashed lines). However, marked differences were found between the two GIT cases #7450 and #328, nicely reflecting the heterogeneity even among GIT with similar genetic background. As can be taken from Figure 1C, the value of both cell types in #7450 (dotted plot) exceeds the mean value, while in #328 (checkered plot) infiltrating cell numbers are far lower than on average.

2.2. Mutational landscape of MLH1$^{-/-}$ tumors

The different tumor spectra detectable in MLH1$^{-/-}$ mice prompted us to perform a whole exome sequencing analysis. This experiment confirmed our observations of high TMB. For the confirmatory analysis, we initially considered all point mutations. TMB ranged from 39 mutations/Megabase (MB) (in GIT #7450) to 943 mutations/MB (in GIT #328). Breaking this down to non-synonymous substitutions, i.e., missense and nonsense mutations, high mutational burden was, by the definition of ref (12) (> 10 mut/MB), preserved, with 3/4 samples even being ultra-hypermutated (> 100 mut/MB) (Figure 2A).

Most mutations in cancer genomes, however, are 'passengers' and do not bear strong imprints of selection. Apart from this, the status of hypermutation complicates the identification of driver mutations simply due to the sheer abundance of somatic variants (13). As MLH1$^{-/-}$-associated lymphomas showed a more aggressive *in vivo* growth behavior and develop considerably earlier than GIT, we expected a different molecular make-up of the lymphomas and possibly also a higher mutational burden. While the former was actually true, the mutational load was not generally higher. Indeed, the lymphomas' mutation rates were highest, but the two GIT cases #7450 and #328 itself differed significantly from each other (Figure 2). The #328s' mutational load was mostly comparable with that of the splenic and skin lymphomas (Figure 2). The very early formation of this GIT before the mean age of onset (~33 weeks for GIT), may explain our finding.

Missense mutations were more frequent than nonsense mutations, and base changes were mainly due to transitions (C>T; A>G) (Figure 2A). High levels of transversion are associated with PD-L1 abundance that functions as a biomarker for immune-checkpoint inhibition. In a previous study, PD-L1 abundance was analyzed on MLH1$^{-/-}$-tumors (14). In line with our recent findings on high percentage numbers of transitions instead of transversions, we also

detected only low-moderate PD-L1 expression (<30 %), and if detectable, this was mainly confined to infiltrating immune cells, see ref. (14).

2.3. Mutation types and shared mutations

Comparative whole exome sequencing of the MLH1$^{-/-}$ GIT #7450 and #328 with the lymphoma revealed the mutanome of these samples (Figures 3 and 4). Considering the number of mutations per type, marked differences were found in the #328 compared to the #7450 GIT and both lymphomas (Figure 3A). As anticipated, the number of silent mutations was high whereas the nonsense mutation rate was low in all four tumor samples. Focusing on the non-synonymous mutations demonstrated similar amounts of these for the #328 GIT and the splenic lymphoma, but slightly increased numbers compared to the skin lymphoma. In fact, #328 from a male mouse had the highest mutation rate in all mutation types, compared to the female counterpart GIT and to the other cancers. Furthermore, lymphomas and GIT shared 640 mutations (Figure 3B), although a high amount of single nucleotide variations (SNV) for each case was exclusive. Interestingly, the lymphomas shared a higher amount of SNV with 684 *vs*. only 10 in the GIT.

In dissecting the mutational landscape (Figure 3C) we initially focused on shared mutations among all cancers most likely functioning as drivers for MLH1-associated tumorigenesis. With this analysis, a surprisingly low number of shared mutations were detectable. These included mutations in the following genes: *AT-rich interaction domain 1A (ARID1A)* and *isocitrate dehydrogenase 2* (*IDH2)*. *ARID1A*, located on chromosome 4, encodes a protein of the SWI/SNF family, contributing to the large ATP-dependent chromatin-remodeling complex. It is an epigenetic modifier that functions as a tumor suppressor; gene mutations have been reported in several malignancies (15). *IDH2* is different, usually being amplified

and/or overexpressed in tumors. Mutations are associated with poor clinical outcome, well reflecting the clinical presentation of biallelic MMR-D-driven malignancies.

2.4. Mutational frequencies and types of alterations for selected gene sets based on prior knowledge in mouse and human

Next, we focused on selected genes with known relevance for tumor initiation and progression as well as tumor suppressive function (Figure 4A). In this analysis and in accordance with the human counterpart, MLH1$^{-/-}$-associated tumors harbor additional mutations in *PIK3CA*, *BRAF* and/or *KRAS* and *ERBB3* (16). Therefore, we created an oncoprint of the non-synonymous alterations in this selected gene set (Figure 4A). A missense mutation was found for *PIK3CA*, *BRAF*, *KRAS*, and *ERBB3*. Events associated with these genes show alterations distributed in a nearly mutually exclusive way across all samples. Surprising are the alterations in the *NF1* gene, a negative regulator of the *RAS* signal transduction pathway that is modified in #328 (primary and cell line). These *NF1* mutations were shown to be concomitant with mutations in the oncogenes *BRAF* or *KRAS* (17,18). Here, the same samples that had *NF1* mutations displayed *BRAF* mutations as well, but only the skin lymphoma and the GIT (#328) had additional *KRAS* mutations. In the case of *APC*, a negative regulator of the *Wnt* signaling pathway (19), we observed for the batch #7450 that the cell line acquired additional missense mutations that had not been detected in the primary. The *PI3K* pathway is affected by *PIK3CA*. Further interactions of *PIK3CA* are with *AKT* and *mTOR* pathways, mutated in one GIT (#328) and both lymphomas. In gastric cancer, *PIK3CA* mutations are associated with a higher aggressiveness (20), while for the lymphomas a strong correlation with *PTEN* mutations is described (21). Both genes were found to be mutated in the GIT (#328) and in splenic lymphoma, respectively. The same was also true for *EGFR* signaling members *ERBB2* and *ERBB3*.

215 *SMAD4* and *POLE* were exclusively detectable in lymphomas (Figure 4A). Of note, the
216 detected somatic *POLE* mutation was located within the exonuclease domain of this gene,
217 executing a proofreading function to decrease the mutation rate during DNA replication. In
218 conjunction with germline MMR-D, *POLE* mutations strongly increase the number of gene
219 mutations in affected tumor cells. Additionally, *SMAD4* acts as a tumor suppressor and
220 inhibits transforming growth factor-β-mediated signaling. Mutations are associated with poor
221 outcome and high metastatic potential. With respect to MLH1$^{-/-}$ tumors, *SMAD4* mutations
222 were constrained to lymphomas.
223

224 **2.5. Pairwise exclusively SNV in GIT and lymphomas**

225 The above data identify different and common mutations among MLH1$^{-/-}$ cancers. We
226 examined the pairwise exclusive mutations among GIT or lymphomas in depth (Figure 3C).
227 While the #328 GIT had fewer mutations per gene, this tumor had generally more genes
228 affected such as *APC*, *PTEN*, *ERBB4*, *IDH1*, *PIK3CA*, *MET*, *BRAF*, *KRAS*, *ERBB3*, *NF1*,
229 *CDC27*, *SOX9*, *MSH3*, *MIER3*, and *RBFOX*. Remarkable is that although both primary
230 tumors have shared genes affected by mutations, the positions of the SNV are exclusive for
231 each of the tumors (shown in red with the corresponding annotation containing the position
232 and the gene, all SNV are in yellow), likely implicating random distribution during
233 oncogenesis.

234 A pairwise comparison of the splenic and skin lymphomas showed that they share the mutated
235 genes *APC*, *SMAD4*, *PTEN*, *ERBB4*, *PIK3CA*, *ARID1A*, *BRAF*, *MET*, *IDH2*, *ERBB3*, *NF1*,
236 and *CDC27*. However, exclusive changes were also observed. Each of the lymphomas has
237 SNV in six exclusive genes. Therefore, we analyzed in detail the processes and functions the
238 exclusively mutated genes are involved in. The splenic lymphoma exhibits SNV in *MYO1B*,
239 *CTNNBL1*, *ERBB2*, *SOX9*, *MSH3*, and *RBFOX1*, involved in cell migration, the spliceosome,

cellular responses, chondrocytes differentiation, and MMR. Exclusive SNV for the skin lymphoma were found in the following genes: *IDH1*, *CASP8*, *ACVR2A*, *KRAS*, *IGF2*, and *POLD1*. All of these genes are part of the electron acceptor, cell apoptosis, oncogene, growth, replication, and repair.

2.6. Prevalence and hotspot regions of GIT and lymphomas in *ARID1A*, *POLE* and *SMAD4*

Mutational hotspots provide more insights into the underlying biology together with the mutations in the domains, such as binding domains. Mutations of major interest for the GIT and lymphomas are appearing in *ARID1A* (Figure 4B). Significant differences between the GIT and lymphomas are the loci of the mutations as well as that more loci are affected in the lymphomas. One amino acid change, D2046N, is located in the SWI/SNF-like complex subunit BAF250/Osa, the ATP-dependent chromatin remodeling complex that regulates gene expression through nucleosome remodeling. Furthermore, the splenic and skin lymphomas share the amino acid changes S571P and P585S. All other mutated loci are found in the putative disordered regions of the *ARID1A* gene.

Figure 4B illustrates the mutational hotspots of the mutually exclusive lymphoma-associated genes *POLE* and *SMAD4*. In *POLE*, we found the shared amino acid change D262Y for the splenic and skin lymphoma. Furthermore, the splenic lymphoma has a nonsense mutation, E265*, in the DNA polymerase B exonuclease domain that adopts a ribonuclease H type fold (22). Interestingly, the lymphomas show an amino acid change, V346I, in the MH2 domain implicated in the control of cell growth (23) of *SMAD4*. Additional loci are in the putative disordered regions, T211A and A229G.

2.7. Somatic mutation distribution and nucleotide changes in chromosome X

In addition to the TMB calculations, we analyzed the mutational load per chromosome. This mutational load was normalized based on the size of the respective chromosome, and the mutation rate per MB plotted for all four entities (supplementary Figure 1). Therefore, this presentation of the chromosomal distribution of SNV shows that for all entities, chromosome 11 accumulated the highest numbers of somatic mutations per MB. Given the fact of differences in gender and a possible hyper-mutation of chromosome X, we investigated chromosome X further for the nucleotide changes in pyrimidines C and T (supplementary Figure 2). C is also responsible for the deamination of the X-chromosome. The coloring of the bars represent the proportions of the six possible nucleotide changes of the pyrimidines (C > A, C > G, C > T, T > A, T > C, and T > G) for chromosome X. Comparing the GIT, we see that T>C is less frequent in the #328 than in the #7450. In turn, the changes C>A and T>G are more frequent. The lymphomas show only minor differences in the nucleotide changes for C>T and T>C, whereby the skin lymphoma had slightly lower changes in this latter than the splenic lymphoma.

2.8. Ongoing mutations in MLH1$^{-/-}$ tumors

To trace the ongoing event of acquiring novel mutations directly, we subsequently compared the mutational profile of selected primary tumors and their corresponding cell line upon *in vitro* culture. As anticipated and in conjunction with observations from clinical CMMR-D samples, numbers of somatic mutations continually increased (Figure 5A). As for the GIT case #7450, which harbors the lowest mutation numbers, TMB more than doubled in the derived cell line. The same was true for coding microsatellite (cMS) mutations, showing a gradual increase during *in vitro* passage (Figure 5B).

Finally, the cMS mutational profile was examined on a panel of primary tumors, i.e. lymphomas and GIT (N = 10 cases each). With this analysis, mutations were detectable in

15/26 markers, with 5 markers being shared among both cancer types (Figure 5C). Of note and of particular relevance, only two genes had the same mutation in their cMS marker of an MSI target gene, thus being in conjunction with our WES data of minor entity-overlapping mutational events. These are *AKT3*, a RAC-gamma serine/threonine-protein kinase with relevance in the maintenance of cellular homeostasis (balancing survival and apoptosis) and the endonuclease *ERCC5* (Excision Repair 5), involved in DNA excision repair. Mutations in this gene increase susceptibility for skin cancer development. Given the biological function of these two genes, their applicability as a target structure is an issue still to be determined.

3. Discussion

Due to the biallelic germline MMR-D and the accordingly complex tumor spectrum, MLH1$^{-/-}$ mice are frequently considered a better model for CMMR-D, instead of Lynch Syndrome. In men, *MLH1* has the highest frequency among monoallelic MMR mutation carriers and also the highest cumulative risk to develop any cancer (24). Despite some differences, MLH1$^{-/-}$ mice combine several key features of both syndromes. The recently detected heterogeneity of Lynch-associated cancers, being highly immunogenic or not (25), additionally argues in favor of using these mice as a model for Lynch Syndrome as well. All malignant human CMMR-D cancers are ultra-hypermutated. However, this is so far not known for tumors arising in the context of Lynch syndrome. Apart from this, there is growing evidence of individual differences between patients, likely being dependent on the underlying MMR defect (26). In line with this broad heterogeneity among MMR-D-related malignancies, we here show that MLH1$^{-/-}$ tumors (I) are either hyper- or ultra-hypermutated, (II) have an entirely individual mutational profile and (III) harbor different mutational hotspots in affected genes.

Of note, along with the different sites of manifestation, a gender-specific prevalence is evident in mice, where thymic lymphomas primarily develop in females, and 80 % of GIT manifest in males. Apart from hormonal-differences, X-chromosome specific alterations may provide a rationale for the different prevalence. The X-chromosome of MLH1$^{-/-}$ mice is indeed highly mutated. However, we could not find evidence for a hypermutated X-chromosome. We could demonstrate that the mutations/MB on the X-chromosome are almost twice compared to the mean mutation rate of the autosomes. Hence, this suggests that the accumulated mutations are coming from the paternal, active X chromosome for the #328 primary tumor and the inactive X chromosome for the #7450 primary tumor. In consequence, this would mean for the lymphomas, that the inheritance of the highly accumulated mutations of chromosome X came from the maternal, active X chromosome. We hypothesize that the high mutation rate on the X chromosome is a cancer-specific feature for the lymphomas and

represents a subgroup in the GIT primary tumors. In addition to the gender, several biological characteristics argue in favor of this hypothesis, leaving technical artifacts as the sole or dominant explanation for the different mutational load very unlikely: (I) the age of onset and (II) the number of tumor-infiltrating lymphocytes.

In the only prior study on the mutational landscapes of MLH1$^{-/-}$ murine tumors, spontaneous as well as irradiation induced T cell lymphomas were analyzed. Results identified many genes commonly mutated but not previously implicated, such as genes involved in NOTCH (e.g. Notch1), and PI3K/AKT (e.g. Pten, Akt2) signaling pathways (10). Our in-depth sequencing analyses adds to these findings and broadens the knowledge on the mutational spectrum of MMR-D related malignancies apart from lymphomas.

By performing in-depth sequencing on lymphomas and GIT, most altered genes involved *APC*, *PTEN*, *PIK3CA*, *Her2*-related genes, *BRAF* and/or *KRAS*. However, it is often difficult to determine, which mutations arose first or whether their order is essential in driving tumorigenesis. While MLH1$^{-/-}$ mice are inbred and all descendants harbor the same germline mutation, we expected a comparable mutational profile among cancers. This was, nevertheless, not the case with a comparably low number of shared mutations among analyzed cancer types. Indeed, entity-overlapping mutations were exclusively detectable in *ARID1A* and *IDH2*. In men, *IDH2* mutations are linked to brain tumors and acute myeloid leukemia, while *IDH1* mutations may drive tumor progression. IDH-mutated tumors are clinically and genetically distinct from their wildtype counterpart. *ARID1A* is a bona fide tumor suppressor and a frequent mutational hotspot in many cancers, including those of the breast, gastrointestinal tract and ovary (27). *ARID1A* functions in MMR regulation, as its loss is associated with MSI. It is supposed to be a driver gene, occurring secondary to MMR-D in gastric cancers, representing an alternative oncogenic pathway to p53 alteration (28). Neither of the tumors examined here showed *TP53* mutations, confirming this assumption. *ARID1A* mutations in MLH1$^{-/-}$-associated tumors are distributed along the entire length of the gene,

thus distinguishing it from typical MSI target genes, a finding also described in the human counterpart (29).

Loss of *ARID1A* shortens time to cancer-specific mortality in men, where mutations are associated with both sporadic and hereditary MSI cancers (30). Though it is still unknown whether CMMR-D cases harbor *ARID1A* mutations as well, this observation fits with our finding on MLH1$^{-/-}$ mice having a significantly shortened life expectancy.

Comparable analysis done by others on human cancers revealed ten overlapping mutations, all of which are InDels involving G7 or C6 repeats (31). These mutations are potentially caused by MSI, and although not analyzed in detail here, we also observed *ARID1A* mutations in our own collection of MMR-D-associated clinical CRC cases (22 % of cases harbor mutations in the G7 repeat and have additionally wildtype *TP53*). *ARID1A* is thus a likely target for personalized medicine in cancer treatment. *ARID1A*-deficiency-based synthetic lethal, targeted drugs are under clinical investigation to suppress cell growth and promote apoptosis (31) (see also *clinicaltrials.gov*). Whether this provides a real opportunity for *ARID1A*-deficient MMR-D-related cancer will need to be tested prospectively.

Another interesting finding of this study was the high prevalence of transitions instead of transversions among gene mutations. Although this is commonly seen in non-smoking associated cancers, we wish to stress the close link between transitions (mainly C-to-T) and MSI as well as *POLE/POLD1* mutations in men (32). While these alterations are detectable in MLH1$^{-/-}$-associated tumors similar mechanisms can be assumed. As for the latter, the relevance of somatic *POLE/POLD1* mutations in the context of MMR-D has only begun to be enlightened. In clinical cases of CMMR-D, most tumors harbor *POLE* mutations affecting the exonuclease domain or domains important to the intrinsic proofreading activity (33). These cells rapidly and catastrophically accumulate point mutations, yielding the ultra-hypermutated phenotype – quite similar to our observations. Cells mutate continuously, raising the question

of how many mutations can be tolerated until a maximum threshold is reached that creates the Achilles' heel.

All mutations described so far may have prognostic, predictive and surveillance potential. Besides, a plethora of low-frequency variants whose functional consequences and clinical actionability are unknown were found as well. We thus conclude that for MLH1$^{-/-}$-driven oncogenesis, many mutations are mere passengers with no functional consequence.

A point worth mentioning is the fact that MMR-D associated lymphomas in men are rarely documented in the literature and most of them develop in patients suffering from CMMR-D. In here, however, hematological malignancies, are common and even in this small group of patients, mostly associated with founder *MLH1* and/or *MSH2* mutations (34). A recent study described the occurrence of MSI/MMR-D in *de novo* Hodgkin lymphoma, but at a significantly higher frequency in Hodgkin's lymphoma survivors developing therapy-related colorectal cancers (35). *MLH1* promoter hypermethylation, but also double somatic mutations are the leading causes of MMR-D (36). Highlighting the relevance of *MLH1,* one study also demonstrates the failure of a specific immune-chemotherapy regimen in follicular lymphoma patients showing *MLH1* gene polymorphisms (37). In addition to germline MMR-D, the frequency of MMR-D arising secondary to anticancer treatment, is thus supposedly higher than previously predicted, considering this a clinically relevant finding. This may finally witness a resurgence of interest to apply and develop alternative therapeutic regimens.

With respect to our study, some neoantigens are auspicious. These include *AKT3, ERCC5* and maybe *ARID1A* as general MMR-D targets, but also *POLE* as lymphoma-specific neoantigen. The finding that this particular mutation was confined to lymphomas may not only explain why this type of malignancies arises earlier in mice than GIT but also represent a target structure worth being included.

Summarizing our findings, we identified a gender-specific aspect in the tumor spectrum, with resulting tumors displaying their own idiosyncratic mutational landscape. The identified shared and mutually exclusive mutations warrant further investigations for therapeutic approaches ideally combined with immune-stimulating and/or -restoring agents.

4. Materials and Methods

4.1. In vivo mouse model & sample acquisition

Homozygous MLH1-deficient mice were bred in the animal facilities (University of Rostock) under specified pathogen-free conditions. Trials were performed in accordance with the German legislation on protection of animals and the Guide for the Care and Use of Laboratory Animals (Institute of Laboratory Animal Resources, National Research Council; NIH Guide, vol.25, no.28, 1996; approval number: LALLF M-V/TSD/7221.3- 1.1-053/12 and 026/17, respectively). Tumor samples for sequencing analysis were obtained from four individual MLH1$^{-/-}$ mice upon spontaneous development. Two mice suffered from a lymphoma (spleen and skin), and the remaining two mice had gastrointestinal tumors both located in the duodenum. All tumors were at an advanced stage at resection. Samples were snap frozen in liquid nitrogen and stored at -80°C. Isolation of gDNA was done by GATC (samples: 7450 primary GIT; A7450 P15 cell line) and CEGAT (samples: 328 primary; 328 cell line; 1351 lymphoma (spleen); 1444 lymphoma (skin)), respectively, prior to the sequencing analyses.

4.2. Whole exome sequencing (WES) analysis.

Data preprocessing: First, the read quality of the raw sequencing data was investigated with FastQC v. 0.11.5 (3) to adjust the adapter trimming. The sequencing adapters were trimmed using Skewer v. 0.2.2 (38), for the reads after demultiplexing with Illumina bcl2fastq v. 2.19. Reads with a Phred quality score ≥ 30 were considered as high quality. The whole-exome reads were mapped to the published mouse genome build ENSEMBL mm10.75 reference using Burroughs Wheeler Aligner (BWA) (39) with the bwa-mem algorithm v. 0.7.2(40). Reads with multiple mappings and the same mapping score have been discarded from further analysis. Additionally, PCR duplicate reads have been removed by using Samtools v. 0.1.18 (39) to prevent artificial coverage brought on by the PCR amplification step during library

preparation and to avoid its impacts on identifying false positive mutations. SNV calling was performed using the Varscan v. 2.4.2 (41), and the detected variants were annotated based on their gene context using snpEff v. 4.3 (42). To compare these data with data from our previously published paper (3), the mm9 SNV coordinates were converted to the corresponding mm10 coordinates with hgliftover v. 30-10-2018 (43,44). The cell line A7450 from the batch was processed likewise (3).

4.3. Data visualization

For the MLH1$^{-/-}$ GIT primary tumor, derived cell line, spleen and skin lymphoma, the summarized mutational profiles with the corresponding mutation type were summarized as stacked bar plot with ggplot2 (45), as Venn diagram with VennDiagram (46) as well as whole-genome ideograms with the circlize (47) R package. Based on the mm10 mouse assembly, provided by the circlize package (47), the filtered mutational profiles are presented as ideograms.

All four different mutational profiles were filtered for the exclusive SNV for each condition separately. Additionally, mutation filters such as the mutation type (missense and nonsense) as well as those mutations occurring in known annotated genes have been applied to mutational profiles.

Additional details like TSTV (transition and transversion) ratio, allele frequency spectrum, base changes, and variant quality for each mutational profile were obtained using the vcf.iobio tool (48).

Furthermore, mapping the mutations and its statistics on a linear gene product (proteins of interest) was done with a ‘lollipop’ mutation diagram generator (49). Based on the knowledge

453 from the human MMR-D counterpart and general involvement in tumorigenesis, the genes for
454 further analysis were chosen with high probability to mutate.

455 *4.4. Hypermutation and TMB calculation*

456 We adopted the following definition for calculating the TMB:

457 $$\frac{\#\ all\ non-synonymous\ SNVs\ on\ target}{covered\ exome\ by\ sequencing\ kit}$$ (50–52).

458 Simply, we used intersectBed from the BEDTools suite v. 2.26.0(53) for ensuring the SNV
459 being on target regions of the Agilent SureSelect Mouse All Exon Kit mm10 and then
460 summing up the number of somatic mutations per MB of the transcriptome mm10 (48.3MB).
461 We use the definition of hypermutation as follows (32,51,52):

462 $$per\ MB_{cancer\ entity} = \begin{cases} hypermutated & if\ non-synonymous\ SNVs > 10 \\ ultra-hypermutated & if\ non-synonymous\ SNVs > 100 \end{cases}$$

463 where $cancer\ entity \in \{GIT, derived\ cell\ line, lymphoma\}$.

464

465 *4.5. Coding microsatellite (cMS) frameshift mutation analysis*

466 Fragment length analysis was done from multiplexed PCRs of gDNA from tumor and normal
467 tissue as described (9). To identify potential MLH1 target genes, a panel (n=26) was screened.
468 Primers were designed using Primer3 software to yield short amplicons (≤200 bp).

469

Acknowledgments

The authors gratefully thank Mrs. Ilona Klamfuss for breeding MLH1 mice.

Conflict of interest. "No potential conflict of interest was reported by the authors."

Author' contributions

YSG: participated in the outline of the manuscript, developed bioinformatics study analysis, performed sequencing data preprocessing, data analysis/interpretation, wrote the manuscript

LW: performed fragment length analysis, participated in *in vivo* data acquisition and data analysis

MH: directed the bioinformatics study analysis, contributed to the discussion and interpretation of the results and paper finalization

AM: participated in literature review and drafted the manuscript

GF: participated in paper finalization and critically revised the manuscript

CJ: participated in paper finalization and critically revised the manuscript

CM: designed study, the outline of the manuscript, performed *in vivo* experiments, data analysis/ interpretation, wrote the manuscript

All authors approved the final version of the paper.

5. References

1. Gupta S, Chatterjee S, Mukherjee A, Mutsuddi M. Whole exome sequencing: Uncovering causal genetic variants for ocular diseases. Experimental Eye Research. 2017.
2. Roche MI, Berg JS. Incidental Findings with Genomic Testing: Implications for Genetic Counseling Practice. Curr Genet Med Rep. 2015;
3. Maletzki C, Gladbach YS, Hamed M, Fuellen G, Semmler M-L, Stenzel J, et al. Cellular vaccination of MLH1−/− mice – an immunotherapeutic proof of concept study. Oncoimmunology. 2018;7(3):e1408748.
4. Boland CR, Goel A. Microsatellite instability in colorectal cancer. Gastroenterology. 2010 Jun;138(6):2073-2087.e3.
5. Ozcan M, Janikovits J, von Knebel Doeberitz M, Kloor M. Complex pattern of immune evasion in MSI colorectal cancer. Oncoimmunology [Internet]. 2018;7(7):1–10. Available from: https://doi.org/10.1080/2162402X.2018.1445453
6. Kloor M, Von Knebel Doeberitz M. The immune biology of microsatellite-unstable cancer. Trends in Cancer [Internet]. 2016;2(3):121–33. Available from: http://dx.doi.org/10.1016/j.trecan.2016.02.004
7. Bakry D, Aronson M, Durno C, Rimawi H, Farah R, Alharbi QK, et al. Genetic and clinical determinants of constitutional mismatch repair deficiency syndrome: Report from the constitutional mismatch repair deficiency consortium. Eur J Cancer [Internet]. 2014;50(5):987–96. Available from: http://dx.doi.org/10.1016/j.ejca.2013.12.005
8. Wimmer K, Rosenbaum T, Messiaen L. Connections between constitutional mismatch repair deficiency syndrome and neurofibromatosis type 1. Clin Genet [Internet]. 2016;(3):507–19. Available from: http://www.ncbi.nlm.nih.gov/pubmed/27779754
9. Maletzki C, Beyrich F, Hühns M, Klar E, Linnebacher M. The mutational profile and infiltration pattern of murine MLH1-/- tumors: concurrences, disparities and cell line

515 establishment for functional analysis. Oncotarget. 2016 Aug;7(33):53583–98.
516 10. Daino K, Ishikawa A, Suga T, Amasaki Y, Kodama Y, Shang Y, et al. Mutational
517 landscape of T-cell lymphoma in mice lacking the DNA mismatch repair gene Mlh1:
518 no synergism with ionizing radiation. Carcinogenesis. 2019;40(2):216–24.
519 11. Maletzki C, Gladbach YS, Hamed M, Fuellen G, Semmler M-L, Stenzel J, et al.
520 Cellular vaccination of MLH1$^{-/-}$mice–an immunotherapeutic proof of concept study.
521 Oncoimmunology. 2018;7(3).
522 12. Campbell BB, Light N, Fabrizio D, Zatzman M, Fuligni F, de Borja R, et al.
523 Comprehensive Analysis of Hypermutation in Human Cancer. Cell. 2017;171(5):1042-
524 1056.e10.
525 13. Martincorena I, Raine KM, Gerstung M, Dawson KJ, Haase K, Van Loo P, et al.
526 Universal Patterns of Selection in Cancer and Somatic Tissues. Cell.
527 2017;171(5):1029-1041.e21.
528 14. Maletzki C, Wiegele L, Nassar I, Stenzel J, Junghanss C. Chemo-immunotherapy
529 improves long-term survival in a preclinical model of MMR-D-related cancer. J
530 Immunother Cancer. 2019;7(1):1–14.
531 15. Ayhan A, Mao T-L, Seckin T, Wu C-H, Guan B, Ogawa H, et al. Loss of ARID1A
532 expression is an early molecular event in tumor progression from ovarian
533 endometriotic cyst to clear cell and endometrioid carcinoma. Int J Gynecol Cancer.
534 2012 Oct;22(8):1310–5.
535 16. Fakhri B, Lim KH. Molecular landscape and sub-classification of gastrointestinal
536 cancers: A review of literature. J Gastrointest Oncol. 2017;8(3):379–86.
537 17. Zenonos K, Kyprianou K. RAS signaling pathways, mutations and their role in
538 colorectal cancer. World J Gastrointest Oncol. 2013 May;5(5):97–101.
539 18. Hayashi T, Desmeules P, Smith RS, Drilon A, Somwar R, Ladanyi M. RASA1 and
540 NF1 are preferentially co-mutated and define a distinct genetic subset of smoking-

associated non–small cell lung carcinomas sensitive to MEK inhibition. Clin Cancer Res. 2018;

19. Sampson EM, Haque ZK, Ku MC, Tevosian SG, Albanese C, Pestell RG, et al. Negative regulation of the Wnt-β-catenin pathway by the transcriptional repressor HBP1. EMBO J. 2001;

20. Kim J-W, Lee HS, Nam KH, Ahn S, Kim JW, Ahn S-H, et al. PIK3CA mutations are associated with increased tumor aggressiveness and Akt activation in gastric cancer. Oncotarget. 2017 Oct;8(53):90948–58.

21. Abubaker J, Bavi PP, Al-Harbi S, Siraj AK, Al-Dayel F, Uddin S, et al. PIK3CA mutations are mutually exclusive with PTEN loss in diffuse large B-cell lymphoma. Leukemia. 2007 Nov;21(11):2368–70.

22. Wang J, Yu P, Lin T, Konigsberg W, Steitz T. Crystal structures of an NH2-terminal fragment of T4 DNA polymerase and its complexes with single-stranded DNA and with divalent metal ions. Biochemistry. 1996 Jun;35(25):8110–9.

23. Yingling JM, Das P, Savage C, Zhang M, Padgett RW, Wang XF. Mammalian dwarfins are phosphorylated in response to transforming growth factor beta and are implicated in control of cell growth. Proc Natl Acad Sci. 1996 Aug;93(17):8940–4.

24. Moller P, Seppala T, Bernstein I, Holinski-Feder E, Sala P, Evans DG, et al. Cancer incidence and survival in Lynch syndrome patients receiving colonoscopic and gynaecological surveillance: first report from the prospective Lynch syndrome database. Gut. 2017 Mar;66(3):464–72.

25. Binder H, Hopp L, Schweiger MR, Hoffmann S, Juhling F, Kerick M, et al. Genomic and transcriptomic heterogeneity of colorectal tumours arising in Lynch syndrome. J Pathol. 2017 Oct;243(2):242–54.

26. Hwang J, Marshall J, Salem M, Grothey A, Goldberg R, Xiu J, et al. O-025Association between tumor mutation burden (TMB) and MLH1, PMS2, MSH2, and MSH6

alterations in 395 microsatellite instability-high (MSI-High) gastrointestinal (GI) tumors. Ann Oncol [Internet]. 2018;29(suppl_5). Available from: https://doi.org/10.1093/annonc/mdy149.024

27. Li M, Hruban RH, Velculescu VE, Bigner D, Goggins M, Kinzler KW, et al. Somatic mutations in the chromatin remodeling gene ARID1A occur in several tumor types. Hum Mutat. 2011;33(1):100–3.

28. Allo G, Bernardini MQ, Wu R-C, Shih I-M, Kalloger S, Pollett A, et al. ARID1A loss correlates with mismatch repair deficiency and intact p53 expression in high-grade endometrial carcinomas. Mod Pathol an Off J United States Can Acad Pathol Inc. 2014 Feb;27(2):255–61.

29. Hänninen UA, Gylfe AE, Renkonen-Sinisalo L, Böhm J, Taipale M, Järvinen H, et al. Exome sequencing reveals frequent inactivating mutations in ARID1A, ARID1B, ARID2 and ARID4A in microsatellite unstable colorectal cancer . Int J Cancer. 2014;135(3):611–23.

30. Bosse T, ter Haar NT, Seeber LM, v Diest PJ, Hes FJ, Vasen HFA, et al. Loss of ARID1A expression and its relationship with PI3K-Akt pathway alterations, TP53 and microsatellite instability in endometrial cancer. Mod Pathol an Off J United States Can Acad Pathol Inc. 2013 Nov;26(11):1525–35.

31. Caumanns JJ, Wisman GBA, Berns K, van der Zee AGJ, de Jong S. ARID1A mutant ovarian clear cell carcinoma: A clear target for synthetic lethal strategies. Biochim Biophys acta Rev cancer. 2018 Dec;1870(2):176–84.

32. Rizvi NA, Hellmann MD, Snyder A, Kvistborg P, Makarov V, Havel JJ, et al. Mutational landscape determines sensitivity to PD-1 blockade in non – small cell lung cancer. 2016;348(6230):124–9.

33. Shlien A, Campbell BB, De Borja R, Alexandrov LB, Merico D, Wedge D, et al. Combined hereditary and somatic mutations of replication error repair genes result in

593 rapid onset of ultra-hypermutated cancers. Nat Genet [Internet]. 2015;47(3):257–62.
594 Available from: http://dx.doi.org/10.1038/ng.3202
595 34. Ripperger T, Schlegelberger B. Acute lymphoblastic leukemia and lymphoma in the
596 context of constitutional mismatch repair deficiency syndrome. Eur J Med Genet
597 [Internet]. 2016;59(3):133–42. Available from:
598 http://dx.doi.org/10.1016/j.ejmg.2015.12.014
599 35. Cuceu C, Colicchio B, Jeandidier E, Junker S, Plassa F, Shim G, et al. Independent
600 mechanisms lead to genomic instability in Hodgkin lymphoma: Microsatellite or
601 chromosomal instability. Cancers (Basel). 2018;10(7).
602 36. Rigter LS, Snaebjornsson P, Rosenberg EH, Atmodimedjo PN, Aleman BM, Ten
603 Hoeve J, et al. Double somatic mutations in mismatch repair genes are frequent in
604 colorectal cancer after Hodgkin's lymphoma treatment. Gut. 2018 Mar;67(3):447–55.
605 37. Rossi D, Bruscaggin A, La Cava P, Galimberti S, Ciabatti E, Luminari S, et al. The
606 genotype of MLH1 identifies a subgroup of follicular lymphoma patients who do not
607 benefit from doxorubicin: FIL-FOLL study. Haematologica. 2015;100(4):517–24.
608 38. Jiang H, Lei R, Ding SW, Zhu S. Skewer: A fast and accurate adapter trimmer for next-
609 generation sequencing paired-end reads. BMC Bioinformatics. 2014;
610 39. Li H, Handsaker B, Wysoker A, Fennell T, Ruan J, Homer N, et al. The Sequence
611 Alignment/Map format and SAMtools. Bioinformatics. 2009;25:2078–9.
612 40. Li H, Durbin R. Fast and accurate short read alignment with Burrows-Wheeler
613 transform. Bioinformatics. 2009 Jul;25(14):1754–60.
614 41. Koboldt DC, Zhang Q, Larson DE, Shen D, McLellan MD, Lin L, et al. VarScan 2:
615 Somatic mutation and copy number alteration discovery in cancer by exome
616 sequencing. Genome Res. 2012;
617 42. Cingolani P, Platts A, Wang LL, Coon M, Nguyen T, Wang L, et al. A program for
618 annotating and predicting the effects of single nucleotide polymorphisms, SnpEff. Fly

(Austin). 2012;

43. Kent WJ, Sugnet CW, Furey TS, Roskin KM, Pringle TH, Zahler AM, et al. The human genome browser at UCSC. Genome Res. 2002;12(6):996–1006.

44. Lander ES, Linton LM, Birren B, Nusbaum C, Zody MC, Baldwin J, et al. Initial sequencing and analysis of the human genome. Nature. 2001;

45. Wickham H. ggplot2. Elegant Graphics for Data Analysis. 2009. 221 p.

46. Chen H, Boutros PC. VennDiagram: a package for the generation of highly-customizable Venn and Euler diagrams in R. BMC Bioinformatics. 2011;12(1):35.

47. Gu Z, Gu L, Eils R, Schlesner M, Brors B. circlize implements and enhances circular visualization in R. Bioinformatics. 2014;30(19):2811–2.

48. Miller CA, Qiao Y, DiSera T, D'Astous B, Marth GT. bam.iobio: a web-based, real-time, sequence alignment file inspector. Nat Meth. 2014 Dec;11(12):1189.

49. Jay JJ, Brouwer C. Lollipops in the Clinic: Information Dense Mutation Plots for Precision Medicine. PLoS One. 2016;

50. Snyder A, Makarov V, Merghoub T, Yuan J, Zaretsky JM, Desrichard A, et al. Genetic Basis for Clinical Response to CTLA-4 Blockade in Melanoma. N Engl J Med. 2014 Dec;371(23):2189–99.

51. Le DT, Uram JN, Wang H, Bartlett BR, Kemberling H, Eyring AD, et al. PD-1 Blockade in Tumors with Mismatch-Repair Deficiency. N Engl J Med. 2015 Jun;372(26):2509–20.

52. Van Allen EM, Miao D, Schilling B, Shukla SA, Blank C, Zimmer L, et al. Genomic correlates of response to CTLA-4 blockade in metastatic melanoma. Science. 2015 Oct;350(6257):207–11.

53. Quinlan AR, Hall IM. BEDTools: a flexible suite of utilities for comparing genomic features. Bioinformatics. 2010;26:841–2.

6. Figure legends

Figure 1: General distribution of tumors in MLH1$^{-/-}$ mice and tumor phenotyping of immunoregulatory markers. (A) Type and frequency of tumors in MLH1$^{-/-}$ mice; data were taken from a total of 90 mice in which spontaneous tumorigenesis was observed. Females were more likely to develop thymic lymphomas, while males were prone to GIT. Generalized splenic lymphomas were found in both genders. **(B)** Flow cytometric phenotyping of MLH1$^{-/-}$ tumors reveals a high abundance of immune-checkpoint molecules on lymphomas. The phenotype of GIT is different with only a few cells expressing these exhaustion markers. Shown data refer to % numbers of cells measured in a live gate on total white blood cells. (**C**) Numbers of tumor-infiltrating lymphocytes in GIT as determined by flow cytometry. Left bar – #7450; middle bar - #328; right bar – mean value of tumor-infiltrating lymphocytes in GIT of MLH1$^{-/-}$ mice. Values are given as percentage of lymphocytes measured from 50.000 events in a live gate. Mean + SD, n=10 mice.

Figure 2: Mutational load and the ratio of non-synonymous mutations compared to all mutations in GIT versus lymphomas. (A) Each bar shows the tumor mutational burden (TMB) per MB for GIT and lymphomas, whereby cases of TMB > 100 are defined as ultra-hypermutated; these are GIT #328 and the lymphomas. Furthermore, in the heatmap, gender, cancer type, and the amount of transitions and transversions are shown in percent. **(B)** The number of mutations in relation to TMB and to the age of onset. Upper graph: all mutations; lower graph: non-synonymous mutations.

Figure 3: Mutational landscape and shared mutations in GIT versus lymphoma. (A) The statistics for each SNV type (missense, nonsense, and silent) are shown for the MLH1$^{-/-}$ GIT primary tumors and the lymphomas including the distribution of the exclusivity of the SNV for each condition. **(B)** The GIT and lymphomas are showing 640 shared SNV in addition to

their exclusive mutations. **(C) Pairwise comparative mutational analysis of MLH1$^{-/-}$ GIT and lymphomas.** Ideogram plots show the genomic distributions of the missense mutations occurring in the annotated/known genes for the MLH1$^{-/-}$ GIT (#7450 and #328, left side). The outermost track (track 0) is the cytoband of the mm10 assembly, followed by four tracks that visualize the SNV belonging to a specific condition (MLH1$^{-/-}$ GIT primary tumors (#7450 and #328, spleen and skin lymphoma). All missense SNV for MLH1$^{-/-}$ GIT primary tumors are blue (#7450, track 1) and yellow (#328, track 3) respectively with their corresponding coordinate on the mouse reference genome mm10 cytoband. The exclusive missense SNV for the MLH1$^{-/-}$ GIT primary tumors are red (tracks 2 and 4) and annotated with a corresponding ID containing the SNV position and the affected gene name. Analogously to for the GIT, the splenic lymphoma (blue) and the skin lymphoma (yellow) are compared for all missense SNV in a pairwise fashion (right side). Red are the exclusive SNV respectively.

Figure 4: Specific cancer-related mutations in GIT and lymphoma. (A) The oncoprint presents genes with tumor suppressive function as well as relevance for tumor initiation and progression. The analysis was done on primary GIT and lymphomas. This visualization provides an overview of the non-synonymous alterations in particular genes (rows) affecting particular individual samples (columns). Red bars indicate missense and blue bars nonsense mutations. **(B) Prevalence and hotspot regions of GIT and lymphomas in *ARID1A*, *POLE*, and *SMAD4*.** Known gene/protein domains are shown in color, other regions in dark grey. Non-synonymous mutations are depicted as nonsense by a blue lollipop and missense by a red lollipop, and a black circle in a lollipop indicates a shared locus of GIT and lymphomas entities. Each lollipop label shows the amino acid change and its location in the amino acid sequence.

Figure 5: Mutational load and the ratio of non-synonymous mutations compared to all mutations in GIT versus the corresponding cell line. **(A)** The barplot shows the tumor mutational burden (TMB) per MB for the GIT and the corresponding cell lines, revealing ultra-hypermutation for GIT #328 and its corresponding cell line (TMB > 100). Furthermore, in the heatmap, gender, cancer type, as well as transitions and transversions are shown in percent. **(B)** Depicted are the percentages of cMS mutations in a panel of MSI target genes originally described in (9). **(C)** Mutation frequency of individual cMS markers among GIT and lymphomas included in this study. Shared mutations were detected in 5/26 totally analyzed markers. Open label – GIT; filled label – lymphoma.

706 **Table 1: Tumor samples included in this study.**

MLH1$^{-/-}$ number	sex	Sample type/origin	Time of onset [weeks]
328	♂	GIT/duodenum	29.5
7450	♀	GIT/duodenum	41.0
1351	♀	Lymphoma/spleen	17.4
1444	♀	Lymphoma/skin	36.0

707 GIT – gastrointestinal tumor.

Supplementary Figure 1: Distribution of somatic mutations in GIT and lymphomas in genomes of female versus male mice. The graph shows the mutational load of non-synonymous mutations on the respective chromosome in the female sample of GIT (#7450) and in the male sample (#328). The mutational load is normalized for the size of the respective chromosome. The coloring of bars indicates the female GIT sample, the male GIT sample and the lymphomas (female, splenic and skin).

Supplementary Figure 2: Distribution of somatic mutations in GIT and lymphomas on chromosome X of female versus male mice. Mutational load of non-synonymous mutations on chromosome X in the female sample of GIT (#7450) and in the male sample (#328). The mutational load of the GIT was compared further to the two female samples of the lymphomas (splenic and skin). Coloring of bars represents the ratio of the six nucleotide changes (C > A, C > G, C > T, T > A, T > C, and T > G) that are most affected by substitutions in the X-chromosome.

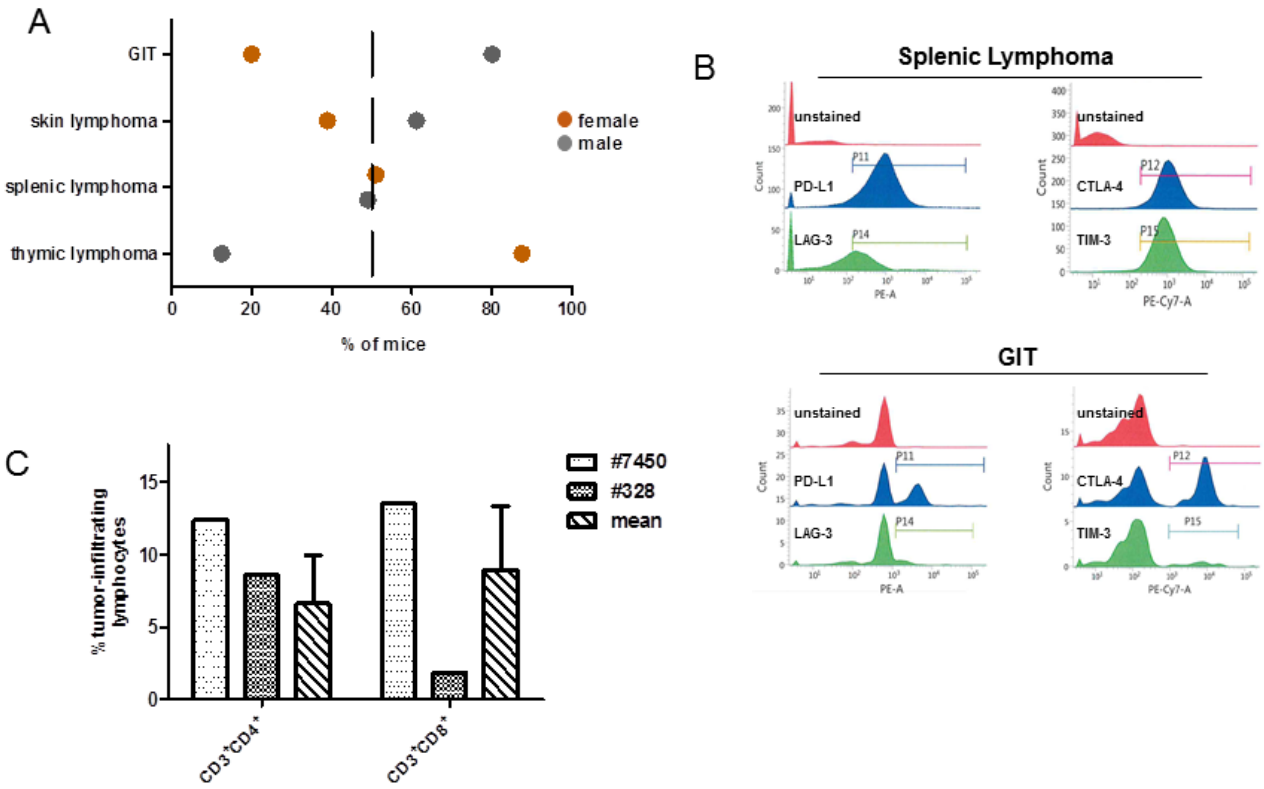
A
GIT
skin lymphoma
splenic lymphoma
thymic lymphoma
female
male
0
20
40
60
80
100
% of mice
B
Splenic Lymphoma
unstained
PD-L1
LAG-3
CTLA-4
TIM-3
P11
P12
P14
P15
PE-A
PE-Cy7-A
Count
GIT
C
% tumor-infiltrating lymphocytes
#7450
#328
mean
CD3+CD4+
CD3+CD8+

Figure 1

723

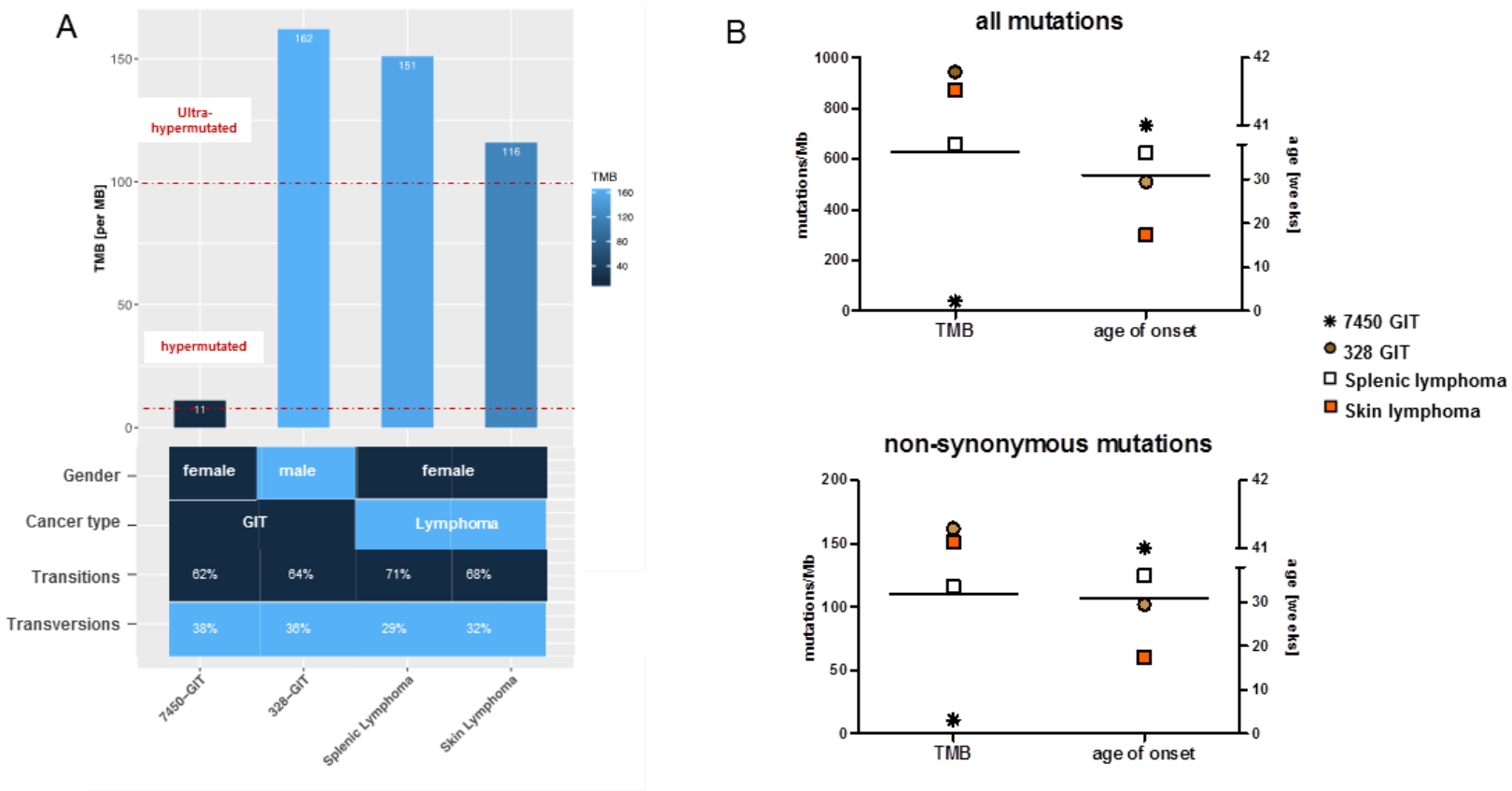
A
TMB [per MB]
150
100
50
0
Ultra-hypermutated
hypermutated
162
151
116
11
TMB
160
120
80
40
Gender
Cancer type
Transitions
Transversions
female
male
female
GIT
Lymphoma
62%
64%
71%
68%
38%
36%
29%
32%
7450–GIT
328–GIT
Splenic Lymphoma
Skin Lymphoma
B
all mutations
mutations/Mb
1000
800
600
400
200
0
age [weeks]
42
41
30
20
10
0
TMB
age of onset
7450 GIT
328 GIT
Splenic lymphoma
Skin lymphoma
non-synonymous mutations
mutations/Mb
200
150
100
50
0
age [weeks]
42
41
30
20
10
0
TMB
age of onset

Figure 2

724

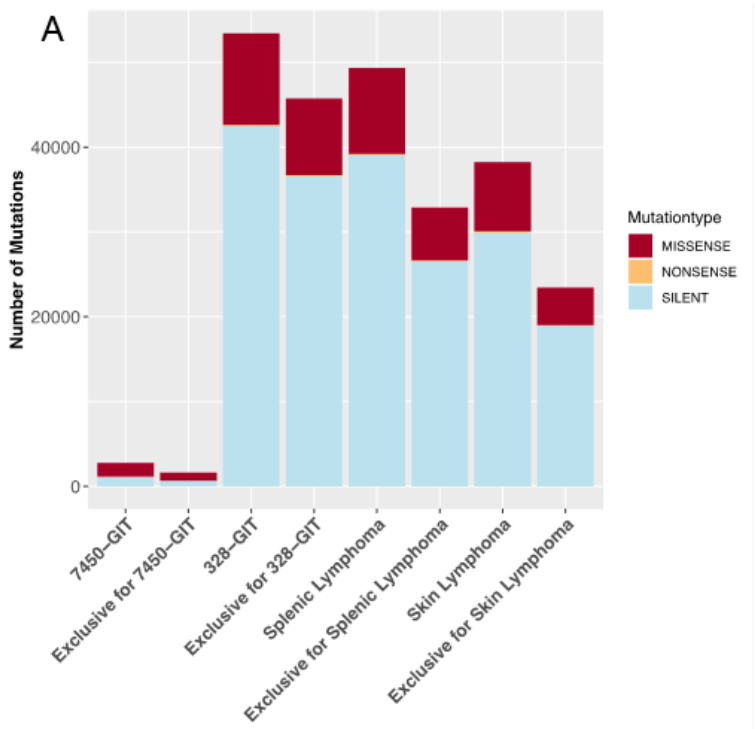
A
Number of Mutations
40000
20000
0
7450−GIT
Exclusive for 7450−GIT
328−GIT
Exclusive for 328−GIT
Splenic Lymphoma
Exclusive for Splenic Lymphoma
Skin Lymphoma
Exclusive for Skin Lymphoma
Mutationtype
MISSENSE
NONSENSE
SILENT

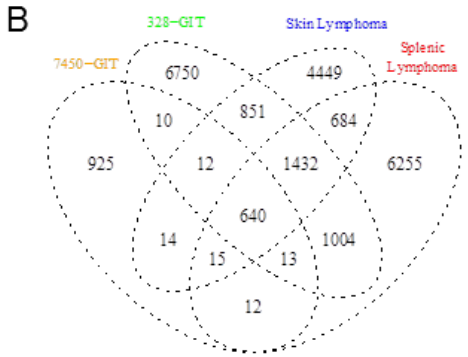
B
7450−GIT
328−GIT
Skin Lymphoma
Splenic Lymphoma
6750
4449
10
851
684
925
12
1432
6255
640
14
15
13
1004
12

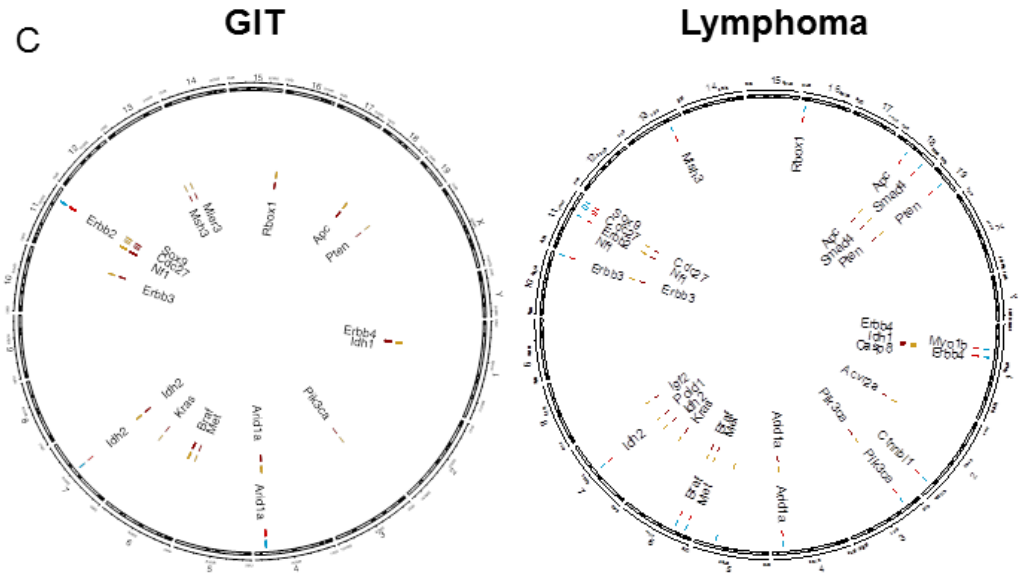
C
GIT
Lymphoma

Figure 3

725

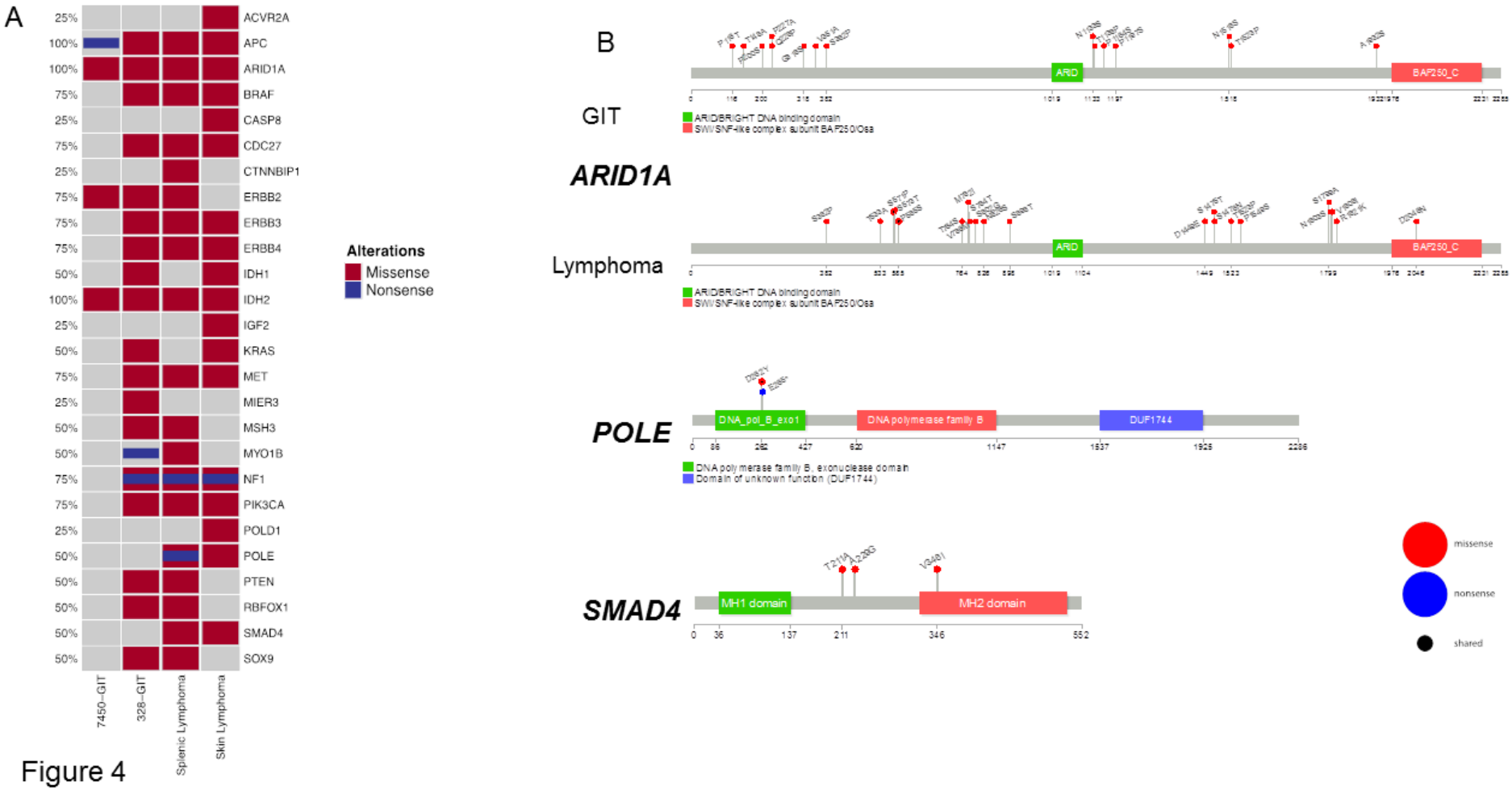
A
25% ACVR2A
100% APC
100% ARID1A
75% BRAF
25% CASP8
75% CDC27
25% CTNNBIP1
75% ERBB2
75% ERBB3
75% ERBB4
50% IDH1
100% IDH2
25% IGF2
50% KRAS
75% MET
25% MIER3
50% MSH3
50% MYO1B
75% NF1
75% PIK3CA
25% POLD1
50% POLE
50% PTEN
50% RBFOX1
50% SMAD4
50% SOX9
7450--GIT
328--GIT
Splenic Lymphoma
Skin Lymphoma
Alterations
Missense
Nonsense
B
GIT
ARID1A
Lymphoma
ARID
BAF250_C
ARID/BRIGHT DNA binding domain
SWI/SNF-like complex subunit BAF250/Osa
POLE
DNA_pol_B_exo1
DNA polymerase family B
DUF1744
DNA polymerase family B, exonuclease domain
Domain of unknown function (DUF1744)
SMAD4
MH1 domain
MH2 domain
missense
nonsense
shared

Figure 4

726

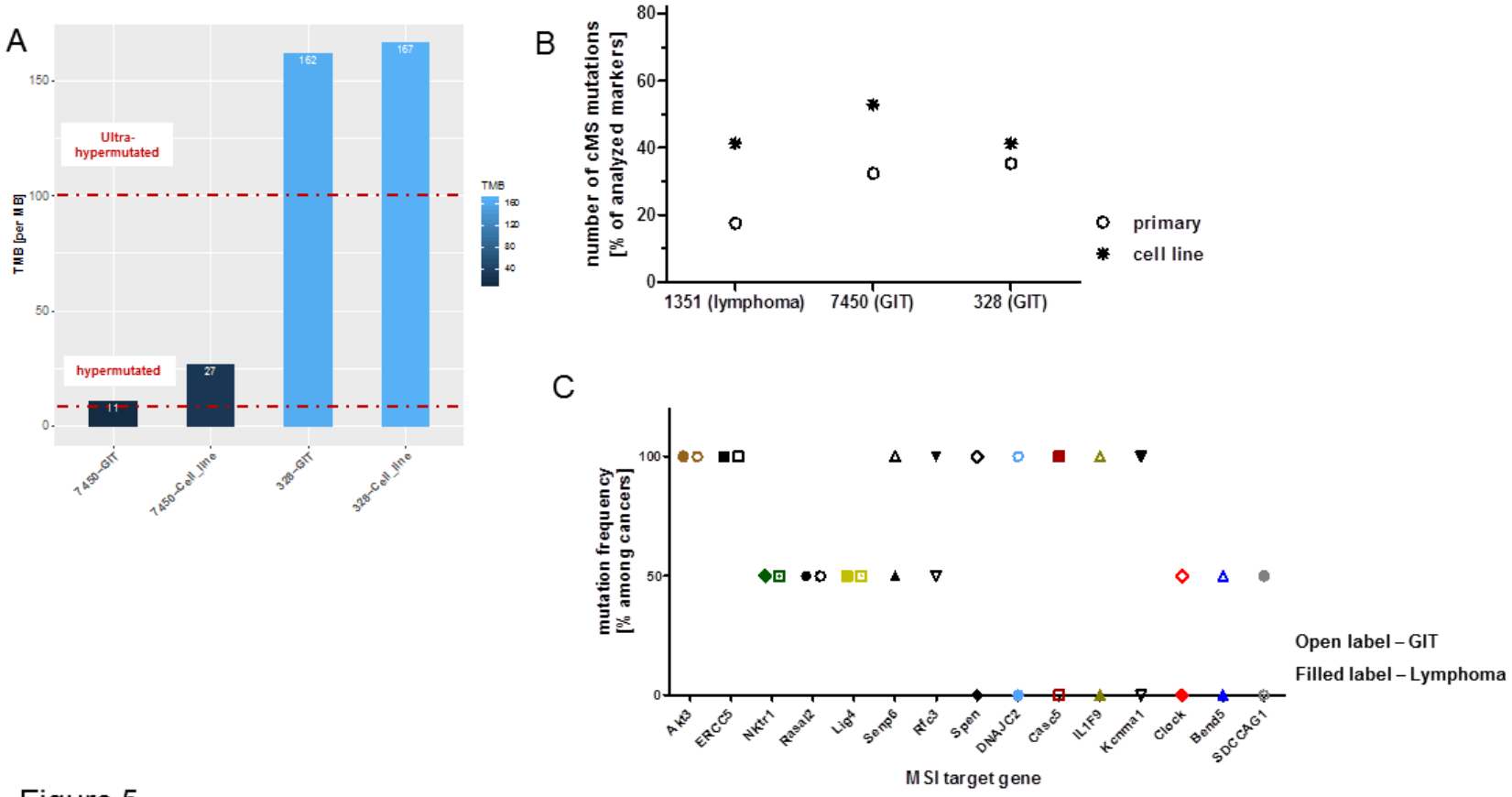
A
Ultra-hypermutated
hypermutated
TMB [per MB]
150
100
50
0
11
27
162
167
TMB
160
120
80
40
7450-GIT
7450-Cell_line
328-GIT
328-Cell_line
B
number of cMS mutations [% of analyzed markers]
80
60
40
20
0
1351 (lymphoma)
7450 (GIT)
328 (GIT)
primary
cell line
C
mutation frequency [% among cancers]
100
50
0
Akt3
ERCC5
NKtr1
Rasal2
Lig4
Semp6
Rfc3
Spen
DNAJC2
Casc5
IL1F9
Kcnma1
Clock
Bend5
SDCCAG1
MSI target gene
Open label – GIT
Filled label – Lymphoma

Figure 5

727

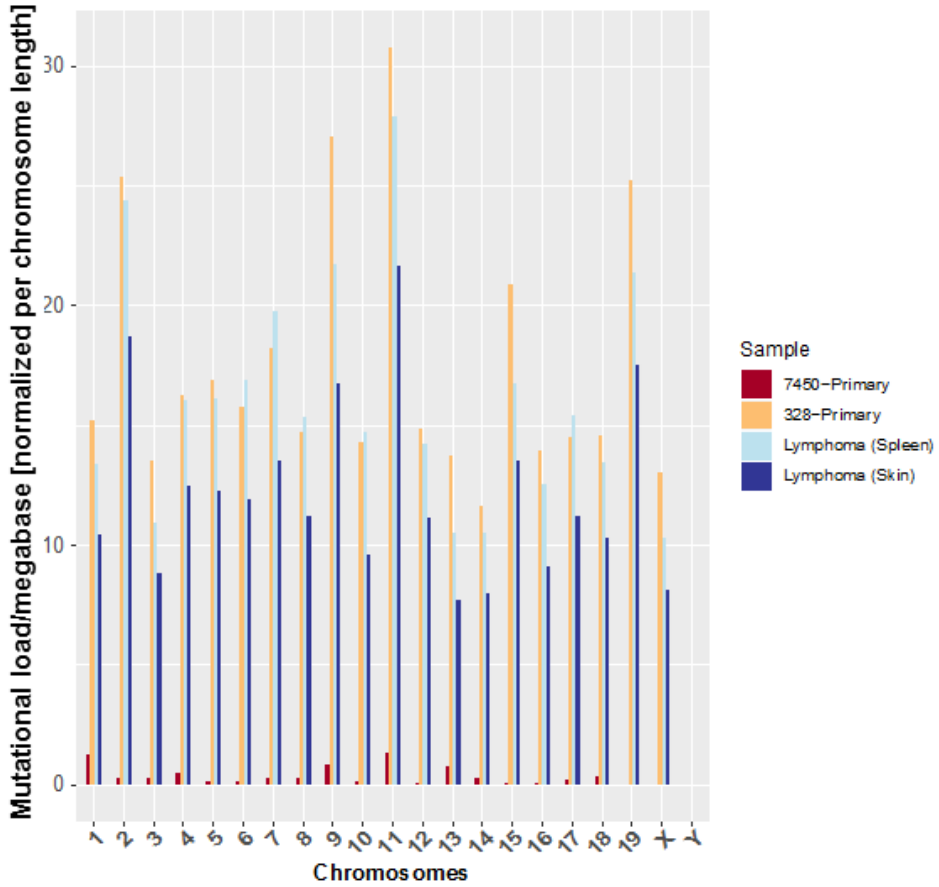

Supplementary Figure 1

728

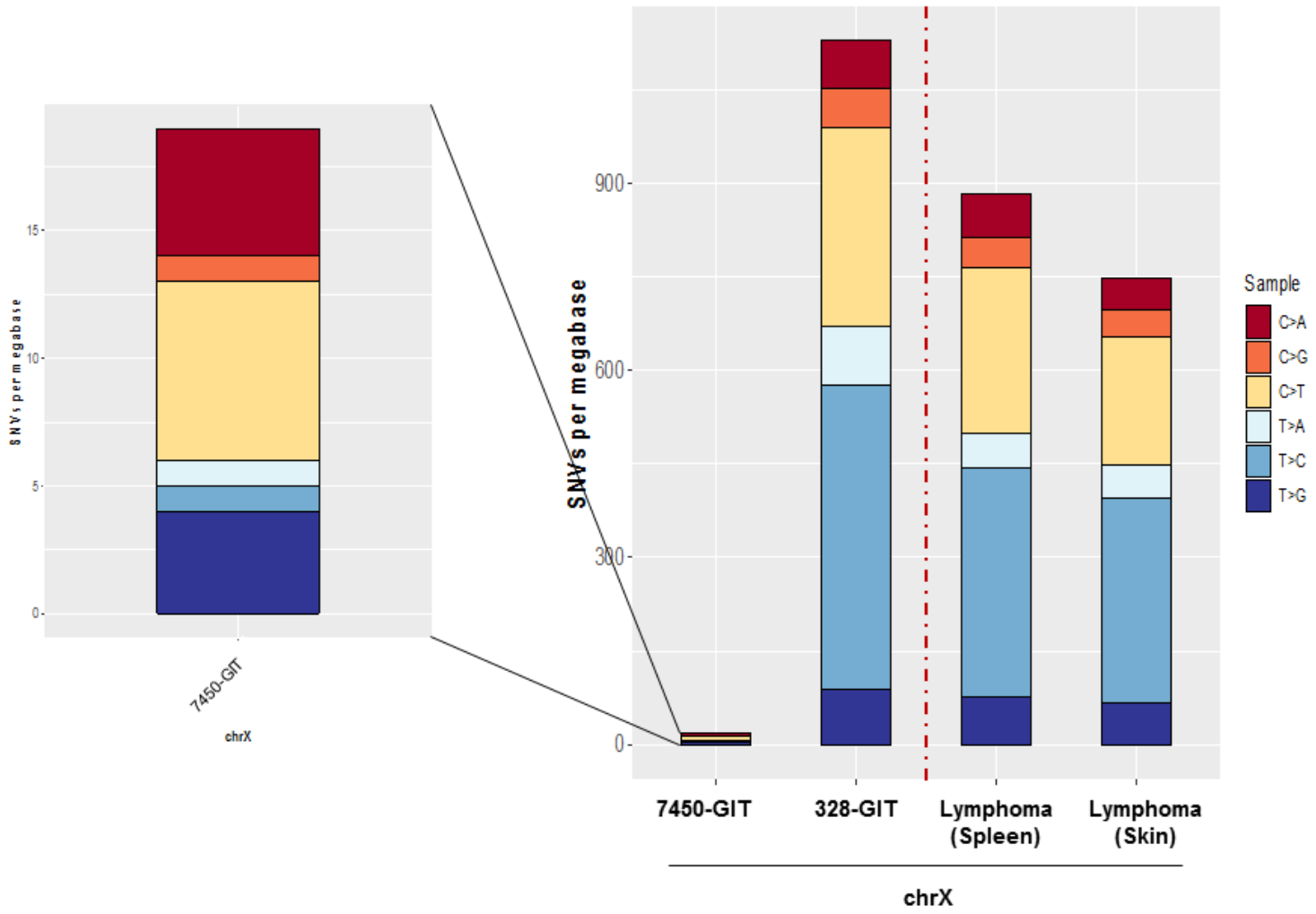

Supplementary Figure 2

729